UNIVERSITY OF TORONTO

Progress Report

by

Jianwei Xu

A report submitted in partial fulfillment for the
degree of Master of Science

in the
Faculty of Arts & Science
Department of Physics

August 2012

UNIVERSITY OF TORONTO

Abstract

Faculty of Arts & Science
Department of Physics

Doctor of Philosophy

by Jianwei Xu

In this report the calculation of tunnelling spectroscopy based on BTK is discussed. Also, we introduce a method of calculating the spectroscopy taking into account proximity effect. Moreover, some additional projects are briefly presented.

Acknowledgements

Thanks for the priceless help from my supervisor, Prof. Ken Burch, and all the people who helped me...

Contents

Chapter 1

Introduction

Tunnelling spectroscopy of superconductors has been a heated topic for a long time. The calculation is based on or the extension of the work of BTK[1] with an assumed step function of pair potential. Extension of the theory, however, is desired due to experimentation[2, 3]. The idea of the approach in the report is that, we first of all find a solution of Bogliubov Equations, then we use the solutions to generate the kernel of the conductance, and once we have the reliable kernel, we could extend our calculation to the required d-wave calculation. One extension discussed by various authors is the d-wave tunnelling spectroscopy based on BTK theory.[4, 5]. Our work is to implement the method to meet our requirements so that this method could fit our experiment data. In this extension, as the kernel has analytical expression, we could skip the solving Bogliubov Equations and start directly the following steps. Another extension is to introduce the proximity effect which is observed in our experimentation. In this extension, we need to walk all the steps stated before. The purpose of the latter project is to approach the c-tunnelling d-wave calculation accounting for the proximity effect.

Chapter 2

Tunnelling Spectroscopy of Superconductors

2.1 Properties of Energy Gaps

The key difference of energy gaps between isotropic superconductor and anisotropic superconductor is their being independent of **k** space and dependent of, respectively.

2.1.1 k Independent Energy Gap of Excited States

We talk about the relationship between energy gap and temperature below in this case, which was discussed in the well known publication, proposing the BCS theory[6]. When we considering $T \neq 0$, it is convenient to introduce free energy

$$F = W - TS \tag{2.1}$$

In the excited states, there will be S_k single particles and P_k pairs in $\Delta_{\mathbf{k}}$, with the rest states occupied by ground states. Therefore we have symbols, $s_k, p_k, 1 - s_k - p_k$ representing the probabilities of excited single particles, excited pairs and group pairs. Hence the diagonal element of $n_{k\sigma}$ is followed by

$$\begin{aligned} &< \psi|n_{k\sigma}|\psi >= \frac{1}{2}s_k + p_k(1 - h_k) + (1 - s_k - p_k)h_k, \epsilon > 0 \\ &< \psi|n_{k\sigma}|\psi >= \frac{1}{2}s_k + p_k h_k + (1 - s_k - p_k)(1 - h_k), \epsilon > 0 \end{aligned} \tag{2.2}$$

Referring to Hamiltonian

$$H_e = \sum_{k>k_F,\sigma} \epsilon_k n_{k\sigma} + \sum_{k<k_F,\sigma} |\epsilon_k|(1 - n_{k\sigma}) - \sum_{k,k'} V_{k,k'} b^*_{k'} b_k \tag{2.3}$$

The average energy

$$W = W_{KE} + W_I \tag{2.4}$$

can be written with the following components

$$W_{KE} = \sum_k |\epsilon_k|[s_k + 2p_k + 2(1 - s_k - 2p_k)h_k|\epsilon_k|] \tag{2.5}$$

and

$$W_I = -\sum_{k,k'} V_{k,k'}[h_k(1 - h_k)h_{k'}(1 - h_{k'})]^{\frac{1}{2}}[(1 - s_k - 2p_k)(1 - s_{k'} - 2p_{k'})] \tag{2.6}$$

By defining that

$$s_k = 2f_k(1 - f_k), p_k = f_k^2 \tag{2.7}$$

where f_k is the fermi distribution. Finally we could write

$$-TS = 2k \sum_k (f_{k'} \ln f_{k'} + (1 - f_{k'}) \ln(1 - f_{k'})) \tag{2.8}$$

Through the free energy we find that

$$\frac{(h_k(1 - h_k))^{\frac{1}{2}}}{1 - 2h_k} = \sum_{k'} \frac{V_{k,k'}(h_{k'}(1 - h_{k'}))^{\frac{1}{2}}(1 - 2f_k)}{2\epsilon_k} \tag{2.9}$$

By introducing the energy gap and acknowledging that we are dealing with isotropic superconductor

$$\Delta = V \sum_{k'} (h_{k'}(1 - h_{k'}))^{\frac{1}{2}} \tag{2.10}$$

where therefore we take the average of interaction independent of k. Solving equation (2.9) and (2.10), we obtain the following important equations

$$h_k = \frac{1}{2}\big[1 - \frac{\epsilon_k}{E_k}\big] \tag{2.11}$$

and

$$E_k = \sqrt{\epsilon_k^2 + \Delta^2} \tag{2.12}$$

We minimise the free energy respect to fermi distribution f_k and replace the sum operation with integral

$$\sum_k = \int N(0) d\epsilon \tag{2.13}$$

where we limit $|\epsilon_k| < \hbar\omega$ as out of this region the interaction will vanish. Finally we obtain the energy gap of isotropic superconductor respect to the temperature

$$\frac{1}{N(0)} = \int_0^{\hbar\omega} \frac{d\epsilon}{\epsilon^2 + \Delta^2} \tanh\left[\frac{1}{2}\beta(\epsilon^2 + \Delta^2)^{\frac{1}{2}}\right], \beta = \frac{1}{kT} \tag{2.14}$$

2.1.2 Energy Gap of Anisotropic Superconductor

In the last section we take an average of the interaction or assume that the interaction is independent of $\mathbf{k}$. We could move forward by replacing this assumption. Assuming that the interaction is only determined by the angel between $\mathbf{k}, \mathbf{k}'$ and expand the interaction accordingly.

$$V_{kk'} = V(\mathbf{k} \cdot \mathbf{k}') = V(\cos\theta_{kk'}) = \sum_l (2l+1) V_l P_l(\cos\theta_{kk'}) \tag{2.15}$$

where

$$V_l = \frac{1}{2} \int_{FS} \frac{d\Omega}{4\pi} V_{kk'} P_l(\cos\theta_{kk'}) \tag{2.16}$$

Notice that the integral is conducted within fermi surface. Using Green function method we could derive that

$$\Delta(\widehat{\mathbf{k}}, T) = \Delta_a(T)\sqrt{4\pi} Y_{lm}(theta_k, \phi_k) \tag{2.17}$$

The average $\Delta_a(T)$ over $\mathbf{k}$ satisfies

$$1 = \frac{1}{2}|V_l| \sum_{k'} \frac{4\pi |Y_{lm}(\widehat{k'})|^2 \tanh(\frac{1}{2}\beta E_{k'})}{E_{k'}} \tag{2.18}$$

where

$$\epsilon_{k'} = \sqrt{E_{k'} + 4\pi\Delta_a^2(T)|Y_{lm}(\widehat{\mathbf{k}})|^2} \tag{2.19}$$

Similar to BCS theory, we replace the sum operator with integral

$$\sum_k = \int d\Omega \int_0^{\hbar\omega} d\epsilon = \int_0^{\pi} \sin\theta d\theta \int_0^{\hbar\omega} d\epsilon \tag{2.20}$$

We could get the equation

$$1 = N(0)|V_L| \int d\Omega \int_0^{\hbar\omega} d\epsilon \frac{4\pi |Y_{lm}(\widehat{k'})|^2 \tanh(\frac{1}{2}\beta E_{k'})}{E_{k'}} \tag{2.21}$$

2.1.3 Energy Gap Terms Selected for the Calculation

In order to simplify the calculation, we skip the implicit relation with temperature of energy gaps, so that only the relation with k space is critical. The relation with temperature is left to be found in fitting the experimental results. Hence for s-wave, we have

$$\Delta = \Delta_0 \tag{2.22}$$

and for d-wave, we have,

$$\Delta = \Delta_0 \cos(2\varphi) \tag{2.23}$$

Their shapes are like

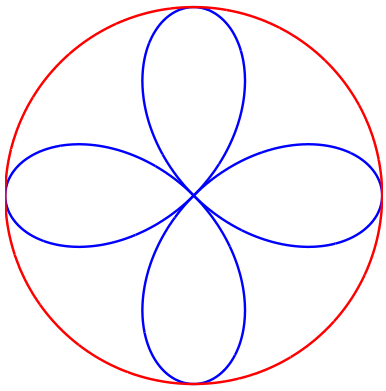

FIGURE 2.1: The shape of s-wave energy gap is a circle while that of d-wave energy gap is like a petal

2.2 Tunnelling Spectroscopy of Superconductors

To approach the calculation of tunnelling spectroscopy of superconductors to fit the experimental results in our group, who is conducting the d-wave experimentation, there are several steps to go in both theory and calculation. First of all, we need to establish the model for s-wave, which, as a matter of fact, is the kernel for the following calculations. Second, with s-wave model established, replacing the term (2.22) with (2.23) when conducting the integral will lead us to the d-wave tunnelling spectroscopy results, in which for sure computing details should be considered. Finally, we obtain the conductance which is the value from the experimentation. Additionally, algorithm for fitting the results need to be implemented. We, however, first of all, introduce the final calculation of conductance respect to bias[1] before we think over on the details of the d-wave tunnelling spectroscopy.

2.2.1 I-V Curve Function For N-S Boundary

This derivation of the function is based on the assumption that all incoming particles are by equilibrium Fermi functions, neglecting the accelerating potential.

With two different distributions for the current of the opposite directions, we have the current

$$I = 2N(0)ev_F\mathcal{A}\int_{-\infty}^{\infty}[f_{\rightarrow}(E) - f_{\leftarrow}(E)]dE \tag{2.24}$$

where we define the following equations

$$f_{\rightarrow}(E) = f_0(E - eV) \tag{2.25}$$

$$f_{\leftarrow}(E) = A(E)[1 - f_{\rightarrow}(-E)] + B(E)f_{\rightarrow}(E) + [C(E) + D(E)]f_0(E) \tag{2.26}$$

Substitute equations(2)(3) into (1) we get

$$I_{NS} = 2N(0)ev_F\mathcal{A}\int_{-\infty}^{\infty}[f_0(E - ev) - f_0(E)][1 + A(E) - B(E)]dE \tag{2.27}$$

where terms A,B,C,D are actually the details we are going to discuss later in this report.

By applying a differential operation on (2.27) we get that

$$\sigma = \int_{-\infty}^{\infty}\sigma_T(E)\frac{\partial f_0(E - eV)}{\partial V}dE \tag{2.28}$$

Omitting the constant factor, the following term is what we are focusing on

$$\sigma_T(E) = 1 + A(E) - B(E) \tag{2.29}$$

where $A(E)$ is the famous Andreev reflection and $B(E)$ is the ordinary reflection, the former of which reflects a hole and generate a Cooper pair in the superconductor side.

2.2.2 *ab*-tunnelling spectroscopy

A simple way for the calculation is to use the following potential model and energy gap model in the NIS junction, where potential is described as a δ function while energy gap step function. Reference [4] indicates a clear way of calculating the *ab*-tunnelling

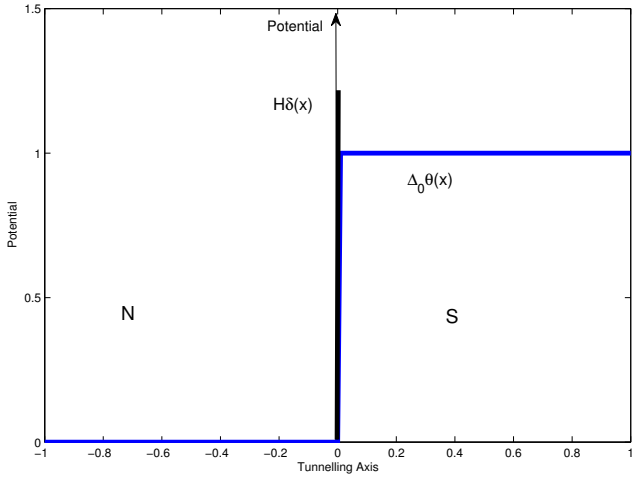

FIGURE 2.2: δ function of potential and step function of energy gap

spectroscopy.

Following the steps stated before, we write the formula for s-wave case

$$\sigma_R(E) = \frac{\sigma_S(E)}{\sigma_N} = \frac{1 + \sigma_N \mid \Gamma_+ \mid^2 + (\sigma_N - 1) \mid \Gamma_+\Gamma_- \mid^2}{\mid 1 + (\sigma_N - 1)\Gamma_+\Gamma_- \exp(i\phi_- - i\phi_+) \mid^2} \tag{2.30}$$

and we write the term $\sigma_S(E)$ for convenience.

$$\sigma_S(E) = \sigma_N \frac{1 + \sigma_N \mid \Gamma_+ \mid^2 + (\sigma_N - 1) \mid \Gamma_+\Gamma_- \mid^2}{\mid 1 + (\sigma_N - 1)\Gamma_+\Gamma_- \exp(i\phi_- - i\phi_+) \mid^2} \tag{2.31}$$

When we set $\phi_- - \phi_+ = 0$, the two energy gaps are always the same. Then we get a figure indicating different shapes with different barrier values, Z.

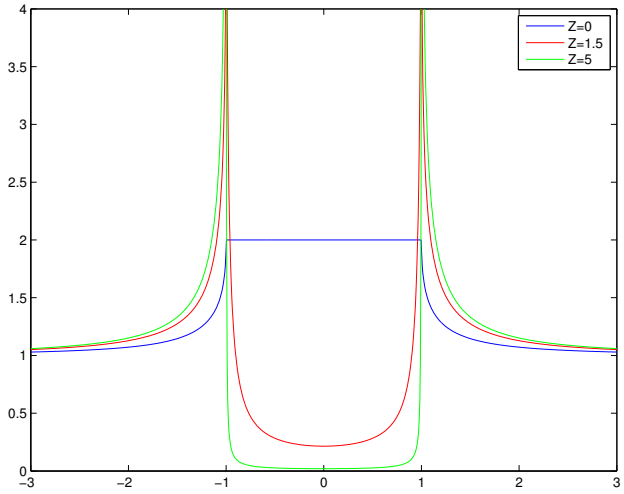

FIGURE 2.3: The picture indicates the different shapes of $\sigma_R(E)$ corresponding to the different barrier values. Here $\Delta_+ = \Delta_-$

The phase difference between the pair potentials Δ_+ felt by electron like particles and Δ_- felt by hole like particles affects the shape of the s-wave spectroscopy significantly.

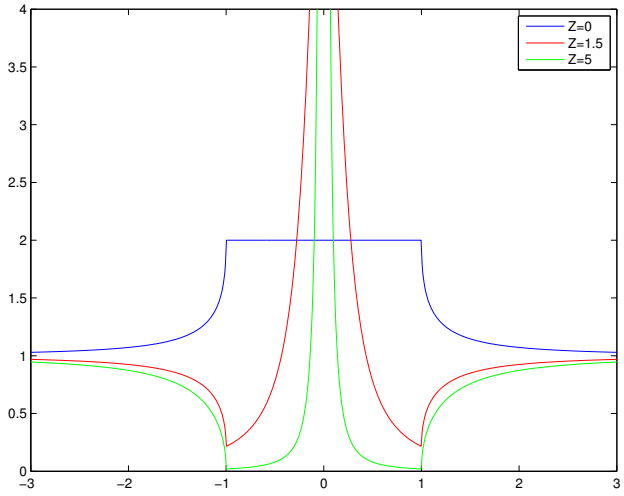

FIGURE 2.4: The picture indicates the different shapes of $\sigma_R(E)$corresponding to the different barrier values. Here $\Delta_+ - \Delta_- = \pi$

We notice that changing the pair potential phase will lead to completely different shapes, , though in the later discussion we always set phase difference as zero.

With s-wave tunnelling spectroscopy obtained, we could now move to d-wave case. The idea is to conduct a solid angel integral after specifying a energy gap term from (2.22) and (2.23), φ in latter of which varies in different cases, that in *ab* tunnelling, φ is

the incident angel θ as the petal of the energy gap is in the incident plain, while in c tunnelling, φ is the angel in the junction interface.

According to the reference[4], the $\sigma_T(E)$ in (2.28) could be written like

$$\sigma_T(E) = \frac{\int_0^{2\pi} d\varphi \int_{-\frac{\pi}{2}}^{\frac{\pi}{2}} d\theta \sigma_S(E) \cos\theta}{\int_0^{2\pi} d\varphi \int_{-\frac{\pi}{2}}^{\frac{\pi}{2}} d\theta \sigma_N \cos\theta} \tag{2.32}$$

A significant feature of this type of tunnelling conductance is that when energy gap amplitude is zero, which turns the material into metal state, is a constant.

Again similar to $\sigma_R(E)$, if we observe the features of $\sigma_S(E)$ according to the angle between the normal axis and the axis of $d_{x^2+y^2}$ petal, named α, the difference of α is actually leading to the difference of phase of the two energy gaps.

Recall that we set energy gap as

$$\Delta_+ = \Delta_0 \cos 2(\theta_N - \alpha) \tag{2.33}$$

$$\Delta_- = \Delta_0 \cos 2(\theta_N + \alpha) \tag{2.34}$$

We show the figure with different α in Fig.2.5.

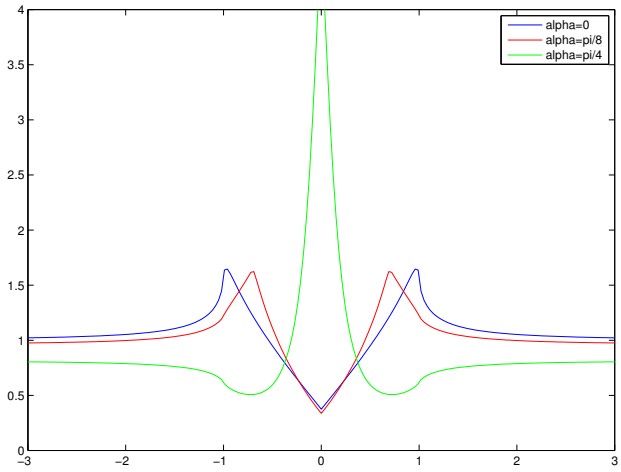

FIGURE 2.5: The figure indicates the correspondence of conductance and angel between incident normal and the petal axis.

The following figure shows the property of the ab tunnelling spectroscopy respect to different pair potential.

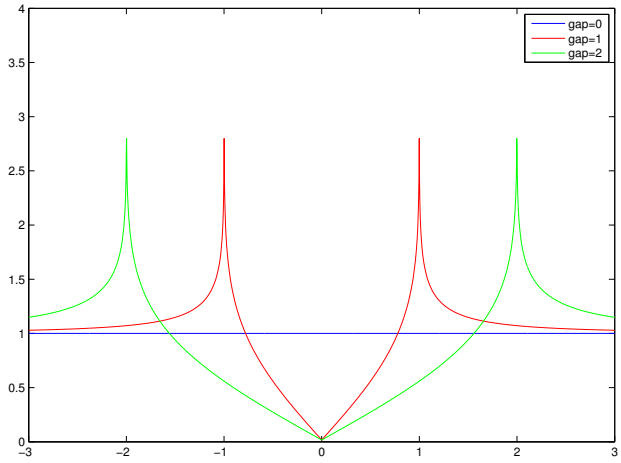

FIGURE 2.6: The figure demonstrates the total tunnelling conductance with different energy gaps. When energy gap amplitude is zero, the peaks vanish, meaning that the material turns into normal metal. Here we choose $Z = 5$

2.2.3 Differential Conductance with Different Temperatures and Fixed Energy Gap Amplitude

In general, the properties of differential conductance is determined by the peak of differential fermi function and tunnelling conductance. As an illustration, we provide a demonstrating Fig.2.7. We see that now the peak of the differential fermi distribution is very sharp, which makes the differential conductance look similar to the tunnelling conductance after the integration, which as a mater of fact, is a convolution.

We plot another figure for furthermore discussion. With T=100K, the differential fermi distribution is rather wider than that of T=1K, leading to the vanish of peaks. The differential fermi function plays a role of broadening the shapes of $\sigma_T(E)$, which is similar to those in Fig.2.6.

A more clear figure is presented in Fig.2.9. The range of temperature is from 1K to 10K, which are indicated by different colours. We could observe that the dip in middle becomes more and more shallow.

2.2.4 Differential Conductance with Different Energy Gap Amplitudes with Fixed Temperature

Though we should be clearly warned that the energy gap is dependent on the temperature, we still do a study for the relation between differential conductance with energy gap amplitudes.

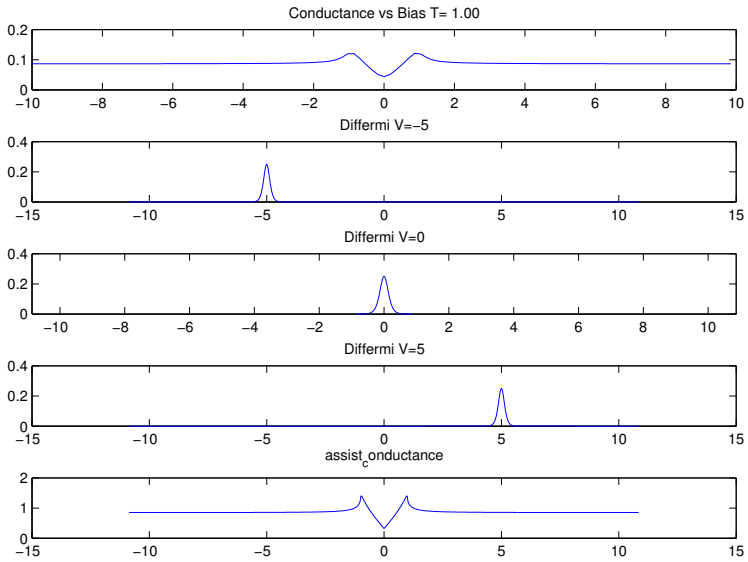

FIGURE 2.7: Differential conductance with T=1K, accompanied by three differential fermi distribution graphs and a tunnelling conductance graph.

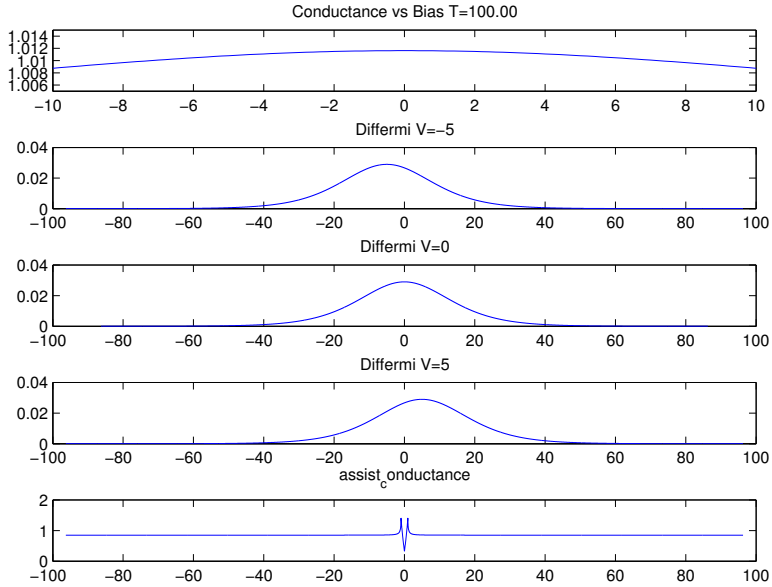

FIGURE 2.8: Differential conductance with T=100K, accompanied by three differential fermi distribution graphs and a tunnelling conductance graph.

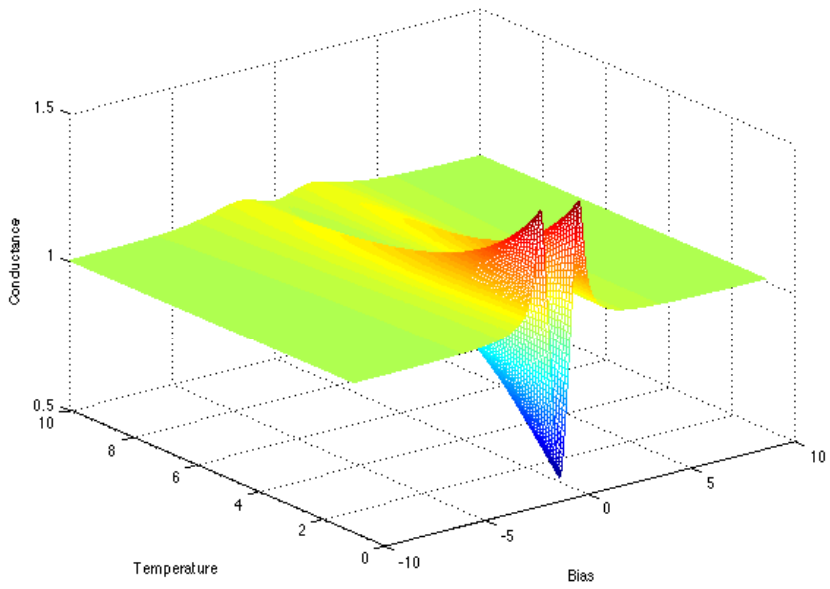

FIGURE 2.9: This figure indicates the relation between temperature, bias and the conductance.The different colours indicate the temperature.

Generally, the shapes of tunnelling conductance are similar except when the energy gap amplitude is zero, which will make the tunnelling conductance constant, already indicated in Fig.2.6.

Therefore, we simply provide an illustration figure. We could notice that with the increase energy gap amplitude, the centre dip becomes deeper.

It should be learned that we are finally try to calculate a second order integral, which may lead a large calculation mission amount. I developed a simple method based on the essential features of function σ_T and differential fermi distribution function $\frac{\partial f_0(E-eV)}{\partial V}$ in the integration (4).

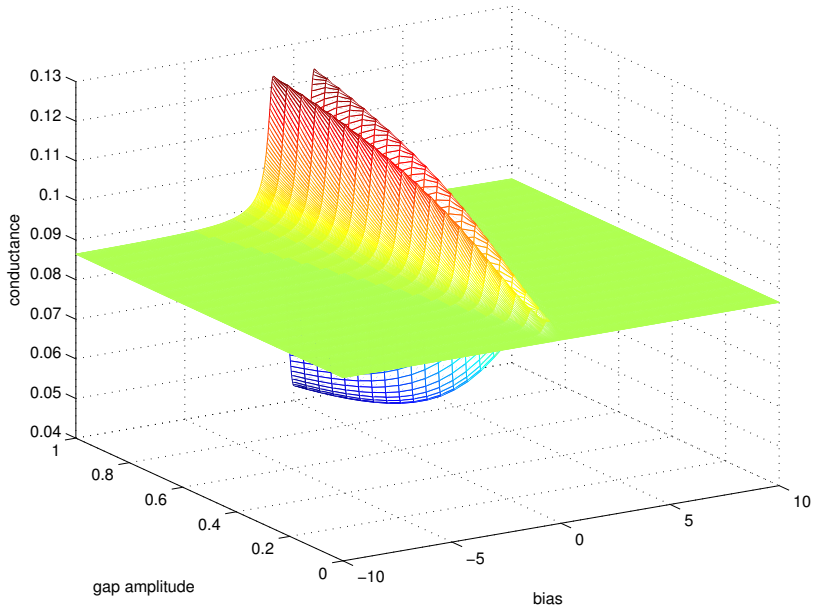

FIGURE 2.10: This figure indicates the relation between energy gap amplitude, bias and the conductance.

First of all, the function $\sigma_T(E)$ becomes CONSTANT when parameter E's abstract value is large compared to the amplitude of energy gap.

Second, it is easily known that differential fermi distribution function is actually of Delta function type, which means the value is zero when its parameter $E - \mu - eV$ is outside a certain range.

Now we set plot step equals to the second integration step chosen, we can obtain fast and accurate integration value. The weakness of this method is that the computation is slow when energy gap amplitude is small while the temperature is high, which, however, is easily to remove by adding some plotting and integrating step boundaries.

2.2.5 *c* tunnelling spectroscopy and fitting the experimental data

As our experiments are conducted with the materials of *c* tunnelling of d-wave pair potential, we now focus on this case. The distinction from the *ab* tunnelling is that the energy gap petal is parallel to the junction interface, leading to the fact that φ in the term (2.23) is the angel in the interface and that we need do an additional integral over φ to complete the solid angel integration; we refer to the formula (2.34) combined with the energy gap (2.23).

The averaged N-I-N junction conductance over the half-sphere of k space could be calculated directed. According to the formula in the following, that calculates the averaged normal conductance,

$$\overline{\sigma_N} = \int_0^{2\pi} d\phi \int_{-\frac{\pi}{2}}^{\frac{\pi}{2}} d\theta \cos\theta \sigma_N \tag{2.35}$$

where we assume that

$$\sigma_N = \frac{1}{1 + (\frac{z}{\cos\theta})^2} \tag{2.36}$$

We could simply calculate the integral for averaged normal conductance,

$$\overline{\sigma_N} = 2\pi\Big(2 - \frac{z^2}{\sqrt{1+z^2}} \ln \frac{\sqrt{1+z^2}+1}{\sqrt{1+z^2}-1}\Big) \tag{2.37}$$

Known the formula (2.37), we could skip the numerical integral of normal conductance. Typically the c tunnelling spectroscopy is similar to that of ab in that they share the same kernel (2.30). The following figure shows the comparison with the reference[4].

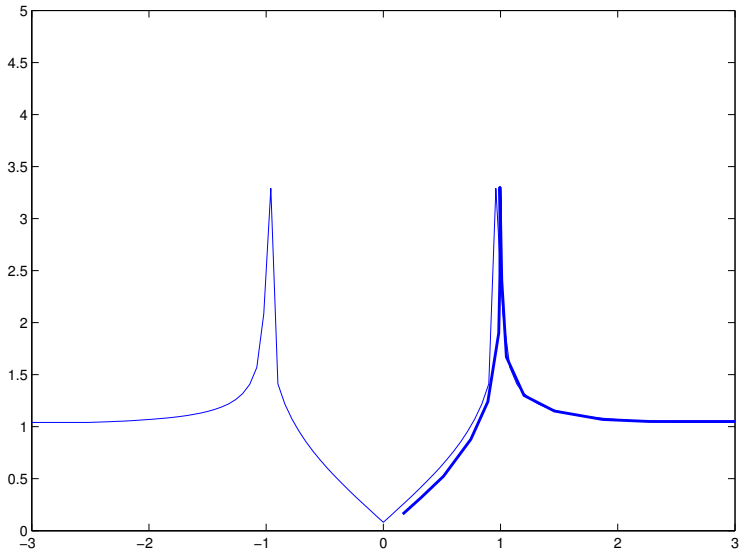

FIGURE 2.11: A simple comparison, where deeper colour represents the digitised data, and $z = 2$

Genetic algorithm is a proper method to approach fitting the data though not implemented. In the calculation, we select a population of 50 for the desired parameters randomly generated within the set range and calculate the fitness value, such as standard error and then sort the population according to the fitness value increasingly.

Second, we choose the first 25 of the population according to the sorted list as parents while we select another 25 samples of the population as mutants randomly multiplied by some restricted random numbers. 25 selected parents will generate 25 offsprings by crossover. Then we mix the original population, the generated offspring as well as the 25 mutants together to compose a country of 100 samples. Third, we do sorting again with the population the eliminate the last 50 samples of the population. We will repeat the above three steps until the termination requirement is satisfied.

The above statement is the ideal approach to fit the experimental data, while unfortunately the results come out not satisfactory. The following results are by done manually.

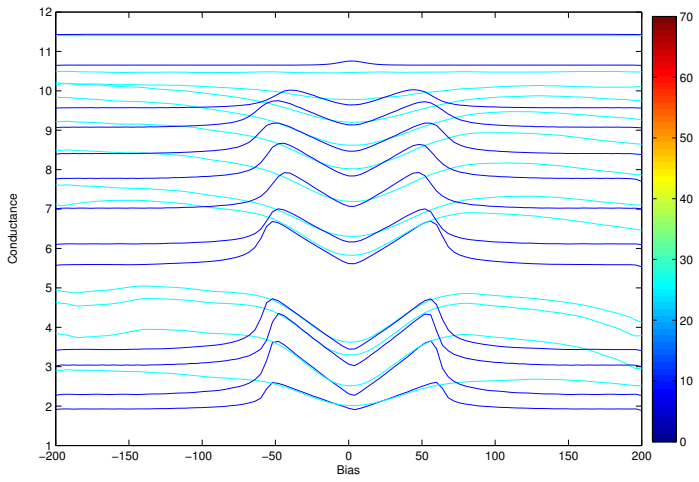

FIGURE 2.12: Conductances with Temperature, where the deep colour represents calculation. Each bundle represents, from bottom to top, sequentially, $10K$,$13K$,$15K$,$21K$,$30K$,$35K$,$40K$,$45K$,$50K$,$55K$,$65K$,$70K$.

And there is energy gap with temperature.

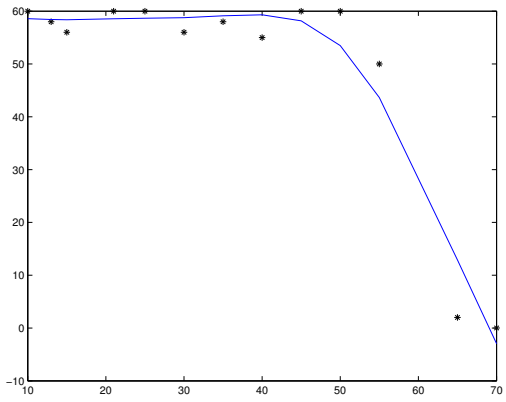

FIGURE 2.13: Energy Gaps with Temperature

Chapter 3

Tunnelling Spectroscopy with Proximity Effect

Our group currently have a featured paper published containing the topic of proximity effect. Hence I am conducting the research trying to analysis the experimental results.

3.1 Bogoliubov Equations

As a matter of fact, the tunnelling conductance discussed in the previous chapter is based on a specific case which is shown in Fig.2.2, where BdG equations have an analytical solution, which in contrast, no longer exists when dealing with more complicated case, such as accounting for proximity effect.

3.1.1 Simplification for Bogoliubov Equations

The general form of the Bogliubov equations are

$$\begin{aligned} i\hbar\frac{\partial f}{\partial t} &= \Big(-\frac{\hbar^2}{2m}\frac{\partial^2}{\partial x^2} - \mu(x) + V(x)\Big) f(x,t) + \Delta(x) g(x,t) \\ i\hbar\frac{\partial g}{\partial t} &= \Big(-\frac{\hbar^2}{2m}\frac{\partial^2}{\partial x^2} - \mu(x) + V(x)\Big) g(x,t) + \Delta(x) f(x,t) \end{aligned} \tag{3.1}$$

who has the solution form

$$\varphi(x,t) = \begin{pmatrix} f(x,t) \\ g(x,t) \end{pmatrix} \tag{3.2}$$

where $\mu(x), \Delta(x), V(x)$ are chemical potential, energy gap, and the ordinary potential which is related to barrier hight, in which we are interested in the latter two. By introducing the solution form

$$\begin{aligned} f &= u(x)e^{ik_F x - \frac{iEt}{\hbar}} \\ g &= v(x)e^{ik_F x - \frac{iEt}{\hbar}} \end{aligned} \tag{3.3}$$

The Bogoliubov equation could be written in this way neglecting higher order term[7].

$$\begin{aligned} \frac{\partial u}{\partial x} &= i(\pi\xi_0\Delta_\infty)^{-1}[Eu - \Delta(x)v] \\ \frac{\partial v}{\partial x} &= -i(\pi\xi_0\Delta_\infty)^{-1}[Ev - \Delta(x)u] \end{aligned} \tag{3.4}$$

which are the equations we are interested in.

3.1.2 A Mathematical Approach to Solve the Equation

Various authors have conducted research on solving the Bogoliubov equations[1, 7]. Here we propose a numerical approach method though not implemented to solve the equations. Let the equations (2.4) have the solution form

$$\phi(x) = \begin{pmatrix} u(x) \\ v(x) \end{pmatrix} \tag{3.5}$$

BdG equations could written in a matrix way,

$$\begin{pmatrix} \frac{d}{dz} & 0 \\ 0 & \frac{d}{dz} \end{pmatrix} \phi = \begin{pmatrix} \beta E & 0 \\ 0 & \beta E \end{pmatrix} \phi + \begin{pmatrix} 0 & -\beta\Delta \\ \beta\Delta & 0 \end{pmatrix} \phi \tag{3.6}$$

in other words,

$$D\phi = (I + M)\phi \tag{3.7}$$

We define an newly introduced solution to the following differential equations,

$$D\phi_0 = I\phi_0 \tag{3.8}$$

which can be easily solved,

$$\phi_0 = \begin{pmatrix} e^{\beta E z} \\ e^{-\beta E z} \end{pmatrix} \tag{3.9}$$

We set that the final solution by introducing a new matrix, which can be easily solved,

$$\phi = P\phi_0 = \begin{pmatrix} p_1 & 0 \\ 0 & p_2 \end{pmatrix} \phi_0 \tag{3.10}$$

We could derive that,

$$D(P\phi_0) = (I + M)(P\phi_0) \tag{3.11}$$

and that,

$$(DP)\phi_0 = (MP)\phi_0 \tag{3.12}$$

Therefore, if we focus on the matrix P, we could reason that,

$$\frac{d}{dz}P = TP \tag{3.13}$$

or

$$\frac{d}{dz}P = \begin{pmatrix} 0 & -\beta\Delta e^{-2\beta E x} \\ \beta\Delta e^{2\beta E x} & 0 \end{pmatrix} P \tag{3.14}$$

An approximated way is to compare to the interaction picture,

$$P = \int TP_0 dz + \int T' dz' \int P' T P_0 dz + \cdots \tag{3.15}$$

We didn't implement this method as we have another clear way clearly indicated by the reference[7]

3.1.3 Solving the Bogliubov Equations

We divide the tunnelling axis into four regions, named 'super','reduced','induced','normal', respectively. In the 'super' region, the solution is written as,

$$\begin{aligned} \varphi_1 &= \begin{pmatrix} u_0 \\ v_0 \end{pmatrix} e^{i(k_F+k_S)x} \\ \varphi_2 &= \begin{pmatrix} v_0 \\ u_0 \end{pmatrix} e^{-i(k_F-k_S)x} \end{aligned} \tag{3.16}$$

where parameters are already known,

$$u_0^2 = 1 - v_0^2 = \frac{1}{2}\Big(1 + \frac{(E^2 - \Delta_\infty^2)^{\frac{1}{2}}}{E}\Big) \tag{3.17}$$

and

$$k_S = (E^2 - \Delta_\infty^2)^{1/2}(\pi\xi_0\Delta_\infty)^{-1} \tag{3.18}$$

The solution of this region serves as the generator of boundary conditions for the solution of the next region,'super'.

$$\begin{aligned} u_{a1}(x_S) &= u_{b2}(x_S) = u_0 e^{ik_S x_S} \\ v_{a1}(x_S) &= v_{b2}(x_S) = v_0 e^{ik_S x_S} \\ u_{b1}(x_S) &= u_{a2}(x_S) = 0 \\ u_{b1}(x_S) &= u_{a2}(x_S) = 0 \end{aligned} \tag{3.19}$$

which is for the solution form of the region 'reduced'.

$$\varphi_j = \begin{pmatrix} u_{aj} \\ v_{aj} \end{pmatrix} e^{ik_F x} + \begin{pmatrix} u_{bj} \\ v_{bj} \end{pmatrix} e^{-ik_F x}, j = 1, 2 \tag{3.20}$$

After obtaining the numerical solutions for (3.20), we select the values of only one point, which is at $x = 0$

$$\begin{aligned} u_{a1}(0) &= u_{b2}(0) = u_{a1}^+ \\ v_{a1}(0) &= v_{b2}(0) = v_{a1}^+ \end{aligned} \tag{3.21}$$

Now we prepare to move into the induced region. First of all we encounter the original boundary condition at $x = 0$, setting $V(x) = Z(\pi\xi_0\Delta_\infty)\delta(x)$.

$$\begin{aligned} \varphi^+ &= \varphi^- \\ \frac{\partial\varphi^+}{\partial x} - \frac{\partial\varphi^-}{\partial x} &= 2k_F Z\varphi^+ \end{aligned} \tag{3.22}$$

We neglect terms $u_{b1}(x), u_{a2}(x), v_{b1}(x), v_{a2}(x)$as they are zero. We now have the boundary conditions for the induced region

$$\begin{aligned} u_{a0}^- = u_{a1}^+, v_{a0}^- = v_{a1}^+ \\ u_{b0}^- = v_{a1}^+, v_{b0}^- = u_{a1}^+ \end{aligned} \tag{3.23}$$

if in the induced region, writing the solution form in the following which will bring to calculation convenience

$$\begin{aligned} \varphi_1 &= (1+iZ)\begin{pmatrix} u_{a0} \\ v_{a0} \end{pmatrix} e^{ik_F x} - iZ\begin{pmatrix} v_{b0} \\ u_{b0} \end{pmatrix} e^{-ik_F x} \\ \varphi_1 &= iZ\begin{pmatrix} u_{b0} \\ v_{b0} \end{pmatrix} e^{ik_F x} + (1-iZ)\begin{pmatrix} v_{a0} \\ u_{a0} \end{pmatrix} e^{-ik_F x} \end{aligned} \tag{3.24}$$

As a remind that these u, v terms are for numerical calculation who all satisfy the Bogliubov equations (3.4) while the terms φ are for mathematical analysis.

After the induced solution numerically solved, we again choose the value only at $x = -x_N$, which is the interface of reduced region and normal region.

$$\begin{aligned} u_a = u_{a0}(-x_N), v_a = v_{a0}(-x_N) \\ u_b = u_{b0}(-x_N), v_b = u_{b0}(-x_N) \end{aligned} \tag{3.25}$$

So that the conductance versus energy is written as

$$T = 1 + A - B = 1 + |a_e|^2 - |b_e|^2 \tag{3.26}$$

where,

$$a_e = \frac{(1+Z^2)u_a v_a - Z^2 u_b v_b}{(1+Z^2)u_a^2 - Z^2 u_b^2} e^{-2ik_N x_N}$$
$$a_e = \frac{iZ(1-iZ)(u_b v_a - u_a v_b)}{(1+Z^2)u_a^2 - Z^2 u_b^2} e^{-2ik_N x_N} \tag{3.27}$$

3.2 Analysis of the Solutions of Bogliubov Equations

3.2.1 The Shapes of Reduced and Induced Pair Potential

To be precise we need to compute the pair potential using self-consistent method[8]. Yet we won't lose two much information if we only guess the shape of the pair potential[3, 7]. We are using parabolic shape of pair potential which is like Fig.3.1

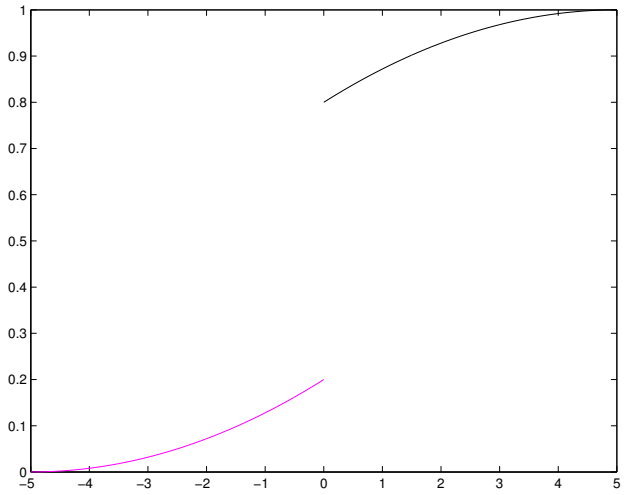

FIGURE 3.1: Parabolic shapes of reduced and induced pair potential

Another point we should account for is the proximity thickness, which will affect much the shape of the computed results. We define

$$x_S = a_S \pi \xi_0, x_N = a_N \pi \xi_0 \tag{3.28}$$

where in effect we find only the factors a_S, a_N play the role of influencing the results. Therefore, we choose the potential function as

$$\begin{aligned} \Delta_R &= \frac{\Delta_+ - \Delta_\infty}{x_S^2}(x - x_S)^2 + \Delta_\infty \\ \Delta_I &= \frac{\Delta_-}{x_N^2}(x + x_S)^2 \end{aligned} \tag{3.29}$$

who have the shapes in Fig.3.1. Now let us first study some intermediate values in the calculation.

3.2.2 Shapes of $|u|, |v|$

We take a look at the shapes of $|u|, |v|$, which are also affected by the chosen energy value E and if not noted, the bulk potential is always set to $\Delta_\infty = 1$

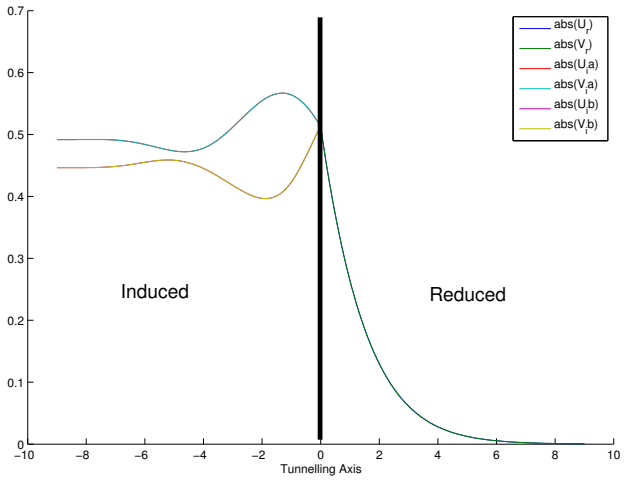

FIGURE 3.2: The shapes with $E = 0.5$, subscript r indicates reduced region while i induced region. Notice that in reduced region, $u^* = v$.

3.2.3 Reproduction the Andreev Reflecion

The calculation until this step agrees quite well with the reference[7]. We reproduce the andreev reflection like in Fig.3.5-3.7

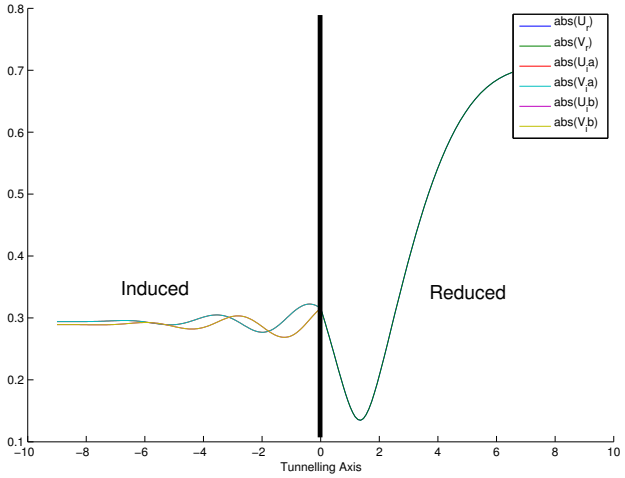

FIGURE 3.3: The shapes with $E = 1$, subscript r indicates reduced region while i induced region

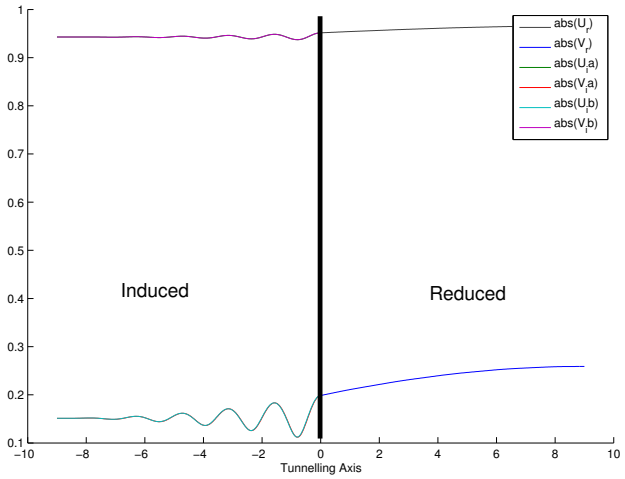

FIGURE 3.4: The shapes with $E = 2$, subscript r indicates reduced region while i induced region

3.2.4 The Specific Case of BTK

Ideally, BTK is a specific case of our discussion in this chapter; in other words, if we set $\Delta_R = 1, \Delta_I = 0$, we should see the results of BTK, Fig3.8. Here are a set of figures, in which the deep blue one represents the BTK, the famous V-shape shown. Also, when barrier hight $Z = 0$, we should observe flat region with the value of 2 in the middle, Fig.3.9.

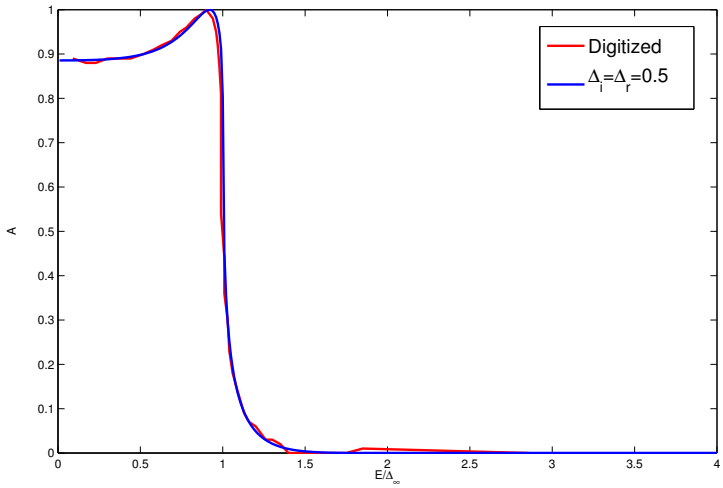

FIGURE 3.5: Andreev reflection with $a_S = a_N = 1.5$ and $Z = 0.3$

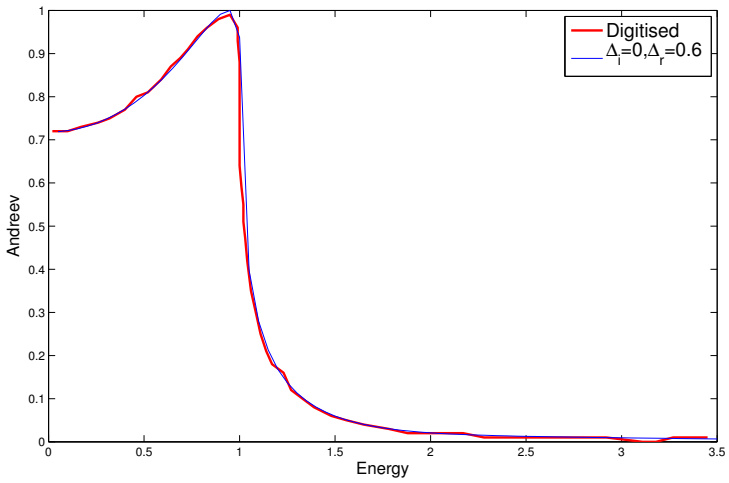

FIGURE 3.6: Andreev reflection with $a_S = a_N = 1.5$ and $Z = 0.3$

3.3 Tunnelling Spectroscopy with Proximity Effect

Similar to the procedure in the previous chapter, with solutions obtained, we first have a look at the kernel of the conductance.

$$\sigma_T = 1 + A - B \tag{3.30}$$

3.3.1 Proximity Effect with various parameters

We draw a list of figures showing the change of the shape according to the different reduced gap and induced gap, setting the coherence length as $\pi\xi_0 = 1$, Fig.3.10, Fig.3.11.

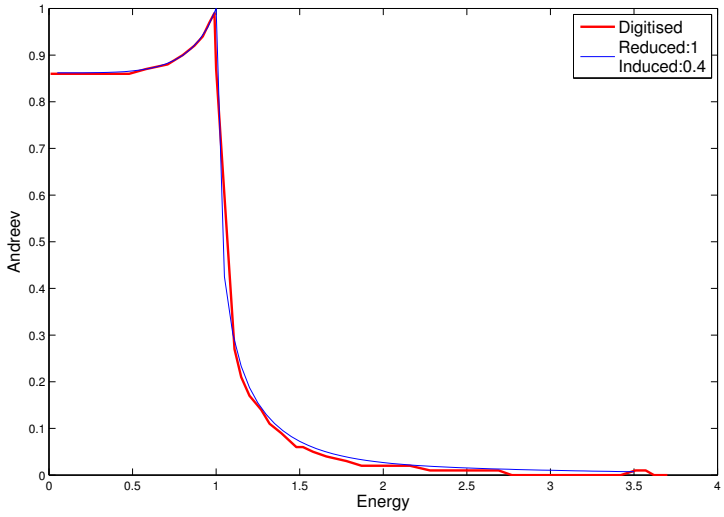

FIGURE 3.7: Andreev reflection with $a_S = a_N = 1.5$ and $Z = 0.3$

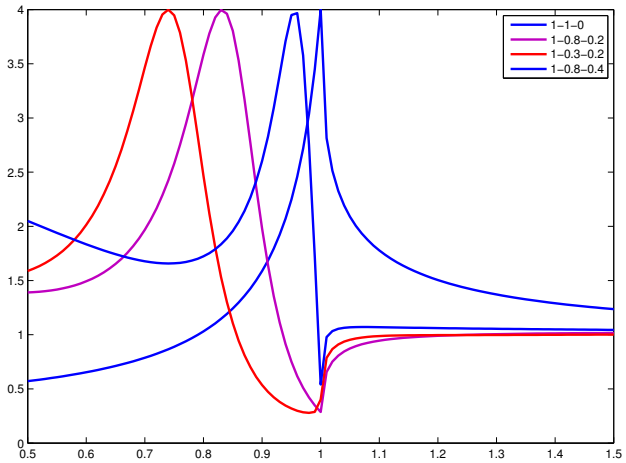

FIGURE 3.8: BTK case titled with $1 - 1 - 0$

In addition, we plot another group of figures with $Z = 0.3$, Fig.3.13, Fig.3.14.

As a thought, the proximity domain certainly affects the behaviours of the transmission. Here I did research on the influences. Fig.3.12 indicates the relationship between proximity domain and the shape of the conductance, with reduced gap 0.8 and induced gap 0.4.

We set the proximity effect parameters as $x_S = x_N = 9, Z = 0.3$, we obtain the Fig.3.16. Their physical meanings, however, remains to be discovered. In this figure, we obtained a number of peaks.

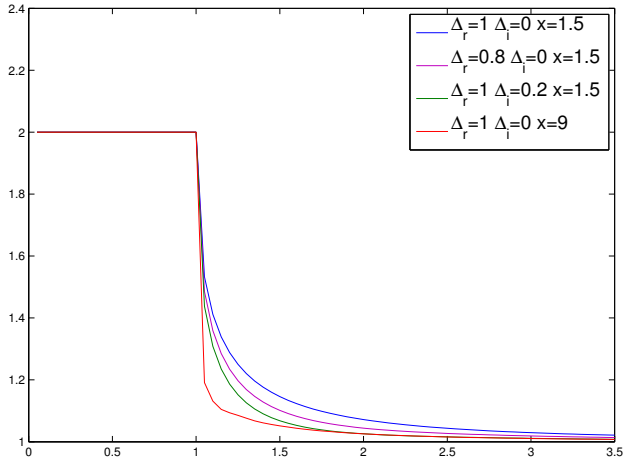

FIGURE 3.9: The flat region in the middle appears no matter what parameters we set

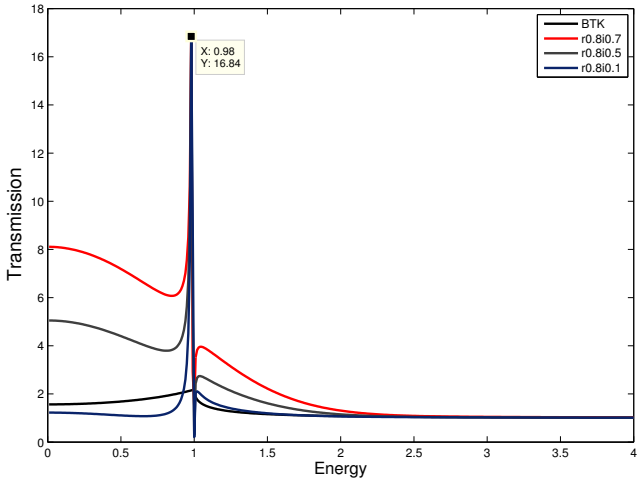

FIGURE 3.10: The figure indicates the difference with induced gap varying.$Z = 3$.

3.3.2 s wave tunnelling spectroscopy with proximity effect

The induced gap brings a bulk in the middle intend of the desired peaks and the function of reduced gap remains unknown. Here we make a small trial step moving to s tunnelling spectroscopy, whose shapes though are analog to those of un-integrated ones. Again we refer to the function, whose plotted picture is shown in Fig.3.17, where we could see the effects of induced gap.

$$\sigma_T(E) = \frac{\int_0^{2\pi} d\varphi \int_{-\frac{\pi}{2}}^{\frac{\pi}{2}} d\theta \sigma_S(E) \cos\theta}{\int_0^{2\pi} d\varphi \int_{-\frac{\pi}{2}}^{\frac{\pi}{2}} d\theta \sigma_N \cos\theta} \tag{3.31}$$

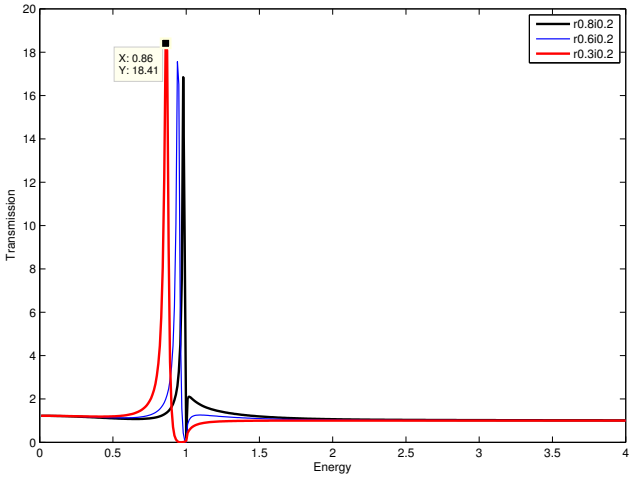

FIGURE 3.11: The figure indicates the difference with reduced gap varying.$Z = 3$

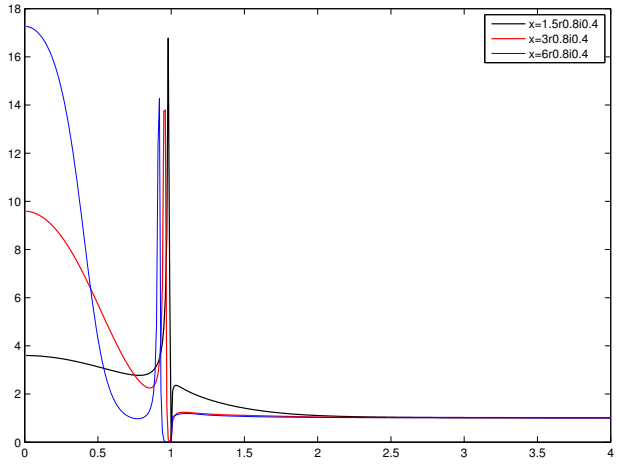

FIGURE 3.12: The proximity domains affects the left side of the shape significantly.$Z = 3$

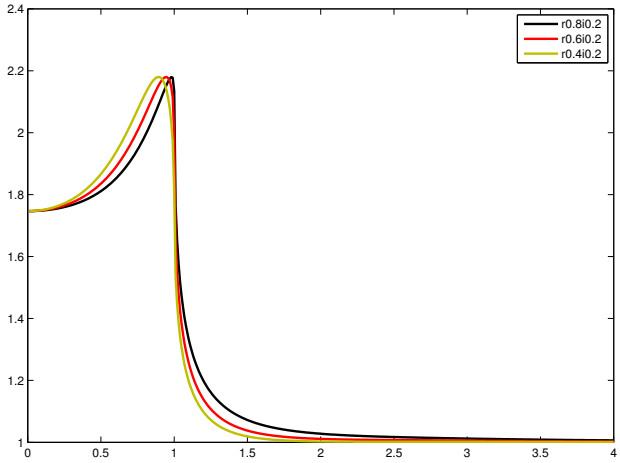

FIGURE 3.13: Low barrier hight.$Z = 0.3$

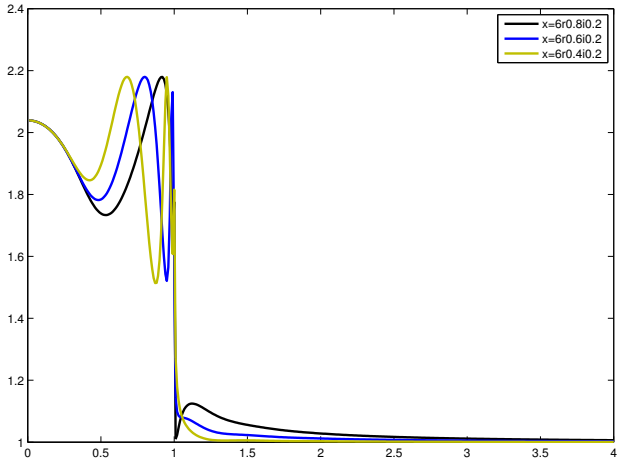

FIGURE 3.14: Some peaks show if thicker proximity domain is chosen at low barrier hight.$Z = 0.3$

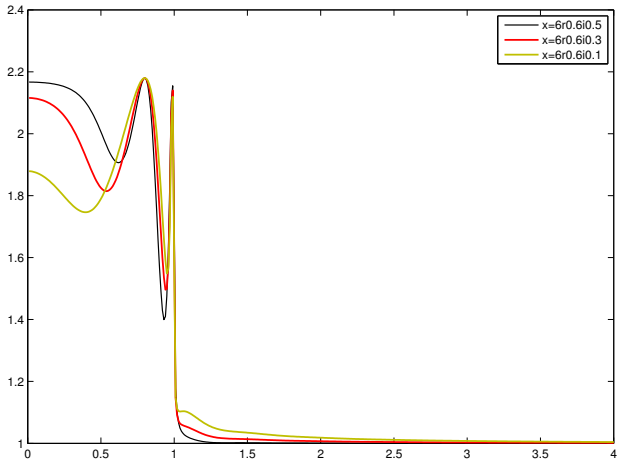

FIGURE 3.15: Some peaks show if thicker proximity domain is chosen at low barrier hight.$Z = 0.3$

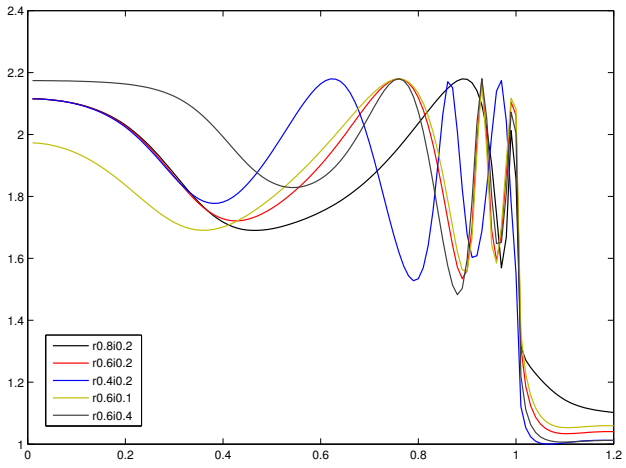

FIGURE 3.16: Some peaks show if thicker proximity domain is chosen at low barrier hight.$Z = 0.3$

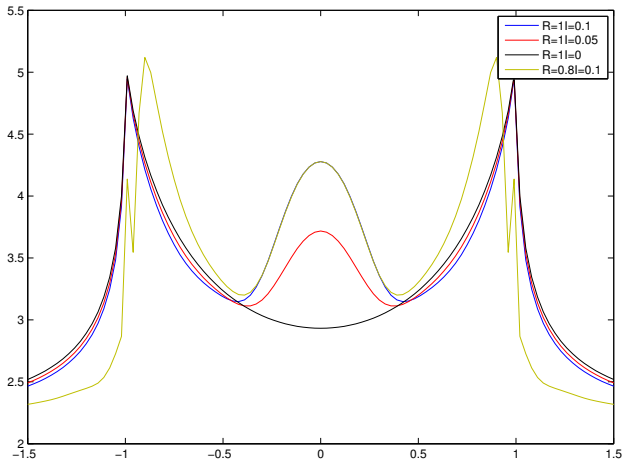

FIGURE 3.17: Some peaks show if thicker proximity domain is chosen at low barrier hight.$Z = 0.3$

Chapter 4

Additional Projects

4.1 Control System for Raman Stage and Fresnel Rhomb

The software I designed integrates the XYZ stage control panel and the Fresnel Rhomb control panel. Users can operate XYZ stage and the Fresnel Rhomb at the same time with convenience. For XYZ stage control part, apart from controlling the stage, users can store the positions of their samples that may be studied later. For Fresnel control part, the digits shown on the software are really polarization angles so that users do not need to convert the units. In addition, a polarization clock is provided to assist the operation. What is more, the COM interface is also adjustable even in the case that the software is installed in a substituted computer.

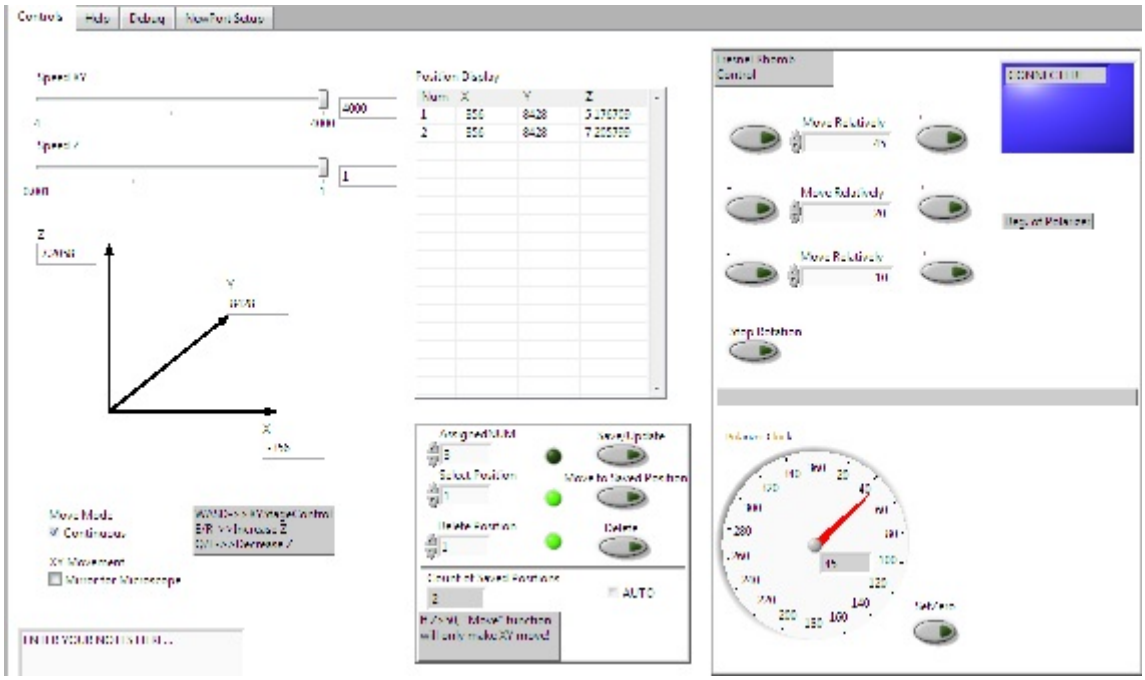

FIGURE 4.1: Main Control Panel

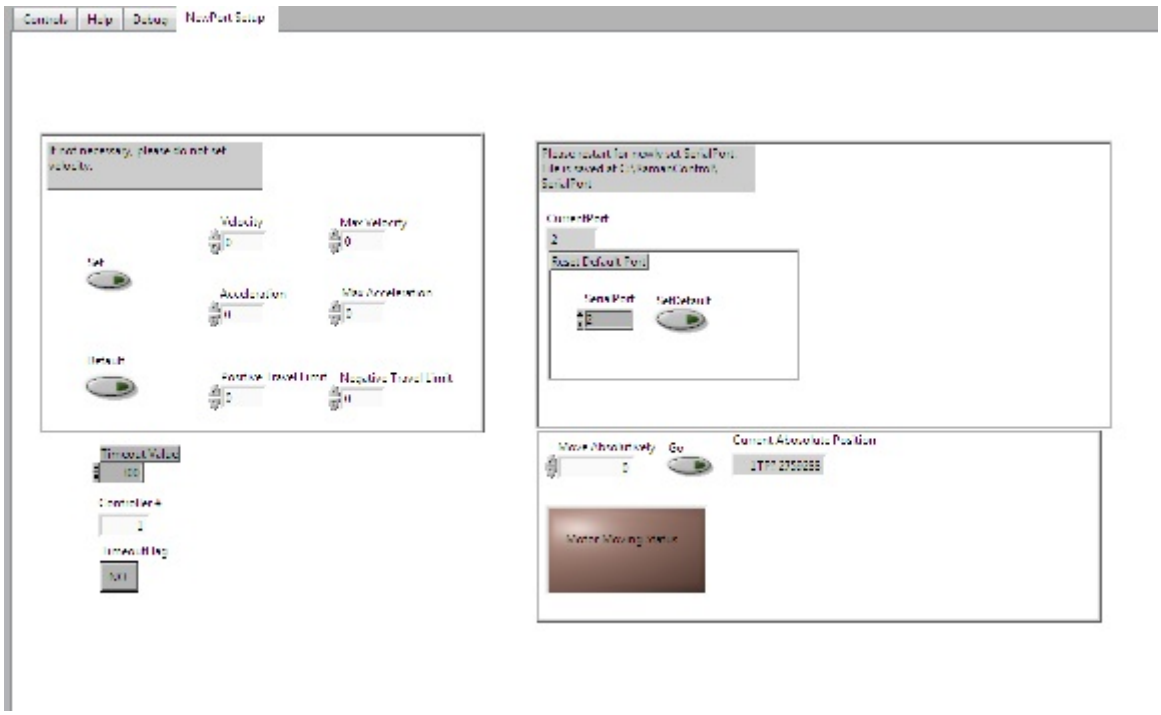

FIGURE 4.2: Setup Control Panel

Bibliography

[1] G. E. Blonder, M. Tinkham, and T. M. Klapwijk. Transition from metallic to tunneling regimes in superconducting microconstrictions: Excess current, charge imbalance, and supercurrent conversion. *Phys. Rev. B*, 25:4515–4532, Apr 1982. doi: 10.1103/PhysRevB.25.4515. URL http://link.aps.org/doi/10.1103/PhysRevB.25.4515.

[2] S. Guéron, H. Pothier, Norman O. Birge, D. Esteve, and M. H. Devoret. Superconducting proximity effect probed on a mesoscopic length scale. *Phys. Rev. Lett.*, 77:3025–3028, Sep 1996. doi: 10.1103/PhysRevLett.77.3025. URL http://link.aps.org/doi/10.1103/PhysRevLett.77.3025.

[3] D. R. Heslinga, S. E. Shafranjuk, H. van Kempen, and T. M. Klapwijk. Observation of double-gap-edge andreev reflection at si/nb interfaces by point-contact spectroscopy. *Phys. Rev. B*, 49:10484–10494, Apr 1994. doi: 10.1103/PhysRevB.49.10484. URL http://link.aps.org/doi/10.1103/PhysRevB.49.10484.

[4] Satoshi Kashiwaya, Yukio Tanaka, Masao Koyanagi, and Koji Kajimura. Theory for tunneling spectroscopy of anisotropic superconductors. *Phys. Rev. B*, 53:2667–2676, Feb 1996. doi: 10.1103/PhysRevB.53.2667. URL http://link.aps.org/doi/10.1103/PhysRevB.53.2667.

[5] Yukio Tanaka and Satoshi Kashiwaya. Theory of tunneling spectroscopy of d-wave superconductors. *Phys. Rev. Lett.*, 74:3451–3454, Apr 1995. doi: 10.1103/PhysRevLett.74.3451. URL http://link.aps.org/doi/10.1103/PhysRevLett.74.3451.

[6] J. Bardeen, L. N. Cooper, and J. R. Schrieffer. Theory of superconductivity. *Phys. Rev.*, 108:1175–1204, Dec 1957. doi: 10.1103/PhysRev.108.1175. URL http://link.aps.org/doi/10.1103/PhysRev.108.1175.

[7] P. C. van Son, H. van Kempen, and P. Wyder. Andreev reflection and geometrical resonance effects for a gradual variation of the pair potential near the normal-metal

˘ superconductor interface. *Phys. Rev. B*, 37:5015–5023, Apr 1988. doi: 10.1103/PhysRevB.37.5015. URL http://link.aps.org/doi/10.1103/PhysRevB.37.5015.

[8] Chr. Bruder. Andreev scattering in anisotropic superconductors. *Phys. Rev. B*, 41: 4017–4032, Mar 1990. doi: 10.1103/PhysRevB.41.4017. URL http://link.aps.org/doi/10.1103/PhysRevB.41.4017.

[9] Chr. Bruder. Andreev scattering in anisotropic superconductors. *Phys. Rev. B*, 41: 4017–4032, Mar 1990. doi: 10.1103/PhysRevB.41.4017. URL http://link.aps.org/doi/10.1103/PhysRevB.41.4017.